$$\mu=3 \quad B=(+1,\ +1,\ +1,\ +1)\ ,$$
$$\mu=4 \quad B=(+1,\ -1,\ -1,\ +1)\ . \qquad \text{(A14)}$$

The transition moment $\vec{M}$ for the unit cell can be obtained from the moments of the four molecules:

$$\vec{M}=\int \Psi^{f} \vec{r}\, \Psi^{0}\, d\tau=\sum_{\alpha} B_{\alpha} \vec{M}_{\alpha}\ , \qquad \text{(A15)}$$

where

$$\vec{M}_{\alpha}=\int \phi_{\alpha}^{f*}\, \vec{r}_{\alpha}\, \phi_{\alpha}^{0}\, d\tau$$

is the transition moment for the α molecule.

If the transition moments transform like vectors and one is known, the other three can be generated by the symmetry operations that transform one molecule to another. $\vec{M}_4$ is obtained from $\vec{M}_1$ and $\vec{M}_2$ from $\vec{M}_3$ by inversion; $\vec{M}_3$ is obtained from $\vec{M}_1$ by a reflection in the ac plane.[10] In terms of the three components of $\vec{M}_1$, the total transition moment will have the following components along the a, b, and c' directions for the four levels:

$$\mu=1 \quad \vec{M}=(0,\ 2M_b,\ 0)\ ,$$
$$\mu=2 \quad \vec{M}=(2M_a,\ 0,\ 2M_{c'})\ , \qquad \text{(A16)}$$
$$\mu=3 \quad \vec{M}=(0,\ 0,\ 0)\ ,$$
$$\mu=4 \quad \vec{M}=(0,\ 0,\ 0)\ .$$

Thus, it is seen that only the first two transitions are allowed and that they will absorb light polarized either parallel or perpendicular to the b axis, respectively. The difference in energy between the two levels at $\vec{k}=0$ is the Davydov splitting.

†Submitted by S. Arnold in partial fulfillment of the requirements for the Ph. D. degree at The City University of New York.

*Supported in part by the U. S. Atomic Energy Commission and the Office of Army Research, Durham, N. C.

[1]P. Avakian and R. E. Merrifield, Mol. Cryst. 5, 37 (1968).

[2]P. Avakian, V. Ern, R. E. Merrifield, and A. Suna, Phys. Rev. 165, 974 (1968).

[3]A. C. Davydov, *Theory of Molecular Excitons* (McGraw-Hill, New York, 1967).

[4]J. Jortner, S. A. Rice, and J. L. Katz, J. Chem. Phys. 42, 309 (1965).

[5]R. H. Clarke and R. E. Hochstrasser, J. Chem. Phys. 46, 4532 (1967).

[6]J. Ferguson, J. Chem. Phys. 28, 765 (1958).

[7]S. Bhagavantam, *Crystal Symmetry and Physical Properties* (Academic, London, 1966), p. 182.

[8]P. Avakian and E. Abramson, J. Chem. Phys. 43, 821 (1965).

[9]R. G. Kepler, J. C. Caris, P. Avakian, and E. Abramson, Phys. Rev. Letters 10, 400 (1963).

[10]J. M. Robertson and J. G. White, J. Chem. Soc. 358 (1947).

[11]R. M. Hochstrasser and S. K. Lower, J. Chem. Phys. 40, 1041 (1964).

[12]R. W. Munn and W. Siebrand, J. Chem. Phys. 52, 47 (1970).

[13]T. Holstein, Ann. Phys. (N. Y.) 8, 343 (1959).

[14]D. S. McClure, in *Solid State Physics*, Vol. 8, edited by F. Seitz and D. Turnbull (Academic, New York, 1959).

[15]D. P. Craig and S. H. Walmsley, in *Physics and Chemistry of the Organic Solid State*, edited by D. Fox, M. M. Labes, and A. Weissberger (Interscience, New York, 1963).

[16]D. P. Craig and S. H. Walmsley, *Excitons in Molecular Crystals* (Benjamin, New York, 1968).

[17]J. Tanaka, Bull. Chem. Soc. Japan 38, 86 (1965).

PHYSICAL REVIEW B VOLUME 3, NUMBER 10 15 MAY 1971

Lattice Dynamics of Rutile*

J. G. Traylor,† H. G. Smith, R. M. Nicklow, and M. K. Wilkinson
Solid State Division, Oak Ridge National Laboratory, Oak Ridge, Tennessee 37830
(Received 30 November 1970)

The phonon dispersion relation for rutile (TiO_2) has been measured by the coherent inelastic scattering of thermal neutrons along principal symmetry directions of the Brillouin zone. Theoretical models based on rigid-ion and shell models, with either axially symmetric or tensor first- and second-neighbor forces, have been fitted to the measured dispersion relation. Only the shell model with tensor forces for all interactions except the second-neighbor oxygen-oxygen interaction was able to give acceptable qualitative agreement with the data, and that agreement is good for only some modes. A frequency distribution and Debye temperature spectrum are presented for that model. The temperature dependence of the frequency of the Γ_1^- (A_{2u}) transverse optic mode is measured from 4 to 300 °K, and the behavior of the square of the frequency is in good agreement with that predicted by the static dielectric constant measurements of Parker.

I. INTRODUCTION

Many of the physical, optical, and chemical properties of a compound are reflected in the lattice dynamics of the crystal. For example, information related to the elastic behavior, specific

heat, dielectric behavior, optical properties, and chemical binding can be obtained from a successful analysis of the measured phonon dispersion relations. Rutile (TiO_2) is of particular interest since more than 20 compounds[1] having interesting magnetic, dielectric, and chemical bonding properties crystallize with this structure; no complete measurement of the phonon dispersion relations has been made[2] for any of these compounds. In addition, rutile has been extensively investigated[3] with studies of the Raman[4,5] and infrared[6,7] active modes at zero-wave-vector elastic constant measurements,[8,9] and determination of the temperature dependence[10] of the static dielectric constants. Cochran[11] discussed the relation of high static dielectric constants and possible "soft" phonon modes, which may lead to ferroelectric phase transitions. In rutile the c-axis static dielectric constant is exceptionally high and demonstrates an increase at low temperatures; therefore, although rutile does not become ferroelectric, the $\Gamma_1^-(A_{2u})$ mode is expected to have an unusually low frequency compared to the behavior of the same mode in other compounds of this structure. With six atoms per primitive unit cell, rutile has 18 branches to its dispersion relations and thus represents one of the most complex structures studied by neutron scattering techniques to date.

The phonon dispersion relations for rutile at 300 °K have been determined experimentally by the coherent inelastic scattering of thermal neutrons. A primary objective of this paper is the presentation of the measured dispersion relations and analyses of those relations in terms of interatomic force models. In particular, the rigid-ion model (which assumes nonpolarizable ions) and the shell model (which allows ionic polarization) are presented, and each is tested with both central forces and tensor forces (as qualified in Sec. II). A secondary objective is the comparison of the temperature dependence of the frequency of the Γ_1^- mode with that of the static dielectric constant along the c axis.

Other workers have attempted to fit the zero-wave-vector frequencies which had been measured by optical experiments. Dayal[12] used a simplified model of central short-range forces. Gubanov and Shur[13] used a rigid-ion model with central forces; however, their assignments of the Raman active modes disagree with the most recent work by Porto *et al.*[4] Katiyar and Krishnan[14] also applied a rigid-ion model with central forces, and were successful in fitting all of the optically active $\vec{q}=0$ frequencies except the Γ_1^- mode. (They concluded that a model which allowed ionic polarization would be required to fit that mode.) However, a present calculation with their parameters is found to give imaginary frequencies for some modes in [110] direction near the Brillouin zone boundary. It is found in this work that both the second-neighbor rigid-ion and shell models, when used with central forces, are unable to predict the qualitative features of the data. The rigid-ion model with tensor forces is also in disagreement with the experiment. Only the shell model with tensor forces is in satisfactory agreement.

II. MODELS

A. Rigid-Ion Model

The rutile structure is primitive tetragonal (D_{4h}^{14}, $P4_2/mnm$) with six atoms per primitive unit cell, as shown in Fig. 1. The two titanium ions occupy positions (000) and $(\frac{1}{2}\frac{1}{2}\frac{1}{2})$, and the four oxygen ions occupy positions ($uu0$), (1-u, 1-u, 0), and $(\frac{1}{2}\pm u, \frac{1}{2}\mp u, \frac{1}{2})$, with the lattice parameters of Table I. The equation of motion is therefore an 18×18 complex matrix equation. We write the equation of motion for the rigid-ion model,[15,16] in which we assume the ions to be point charges, as

$$\underline{M}\,\omega^2\,\underline{U} = (\underline{R}+\underline{Z}\underline{C}\underline{Z})\,\underline{U}\,, \tag{1}$$

where $\underline{M}$ is a diagonal matrix of atomic masses, ω^2 is a diagonal matrix of squares of the circular frequencies of vibration, $\underline{U}$ is a matrix composed of displacement vectors of the ions, $\underline{R}$ is a matrix specifying the short-range interactions, $\underline{Z}$ is a diagonal matrix of ionic charges, and $\underline{C}$ is the matrix of Coulomb coefficients.[17]

The short-range interaction matrix $\underline{R}$ is of the form

$$R_{\alpha\beta}^{\kappa\kappa'}(\vec{q}) = \sum_{l'} \Phi_{\alpha\beta}(0\kappa, l'\kappa') e^{-i\vec{q}\cdot[\vec{r}(0\kappa)-\vec{r}(l'\kappa')]}\,, \tag{2}$$

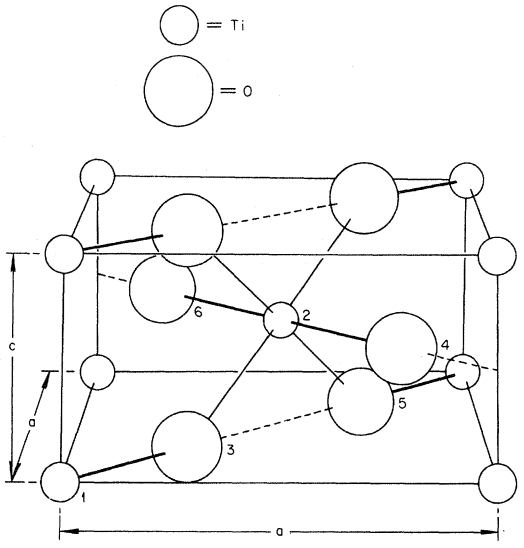

FIG. 1. Rutile structure.

TABLE I. Physical properties of rutile at room temperature.

Property	Quantity		Unit
Lattice parameters[a]	$a = 4.593\,73$		Å
	$c = 2.958\,12$		Å
	$u = 0.305\,6$		dimensionless
Elastic constants[b]	$C_{11} = 2.660 \pm 0.066$		10^{12} dyn/cm^2
	$C_{12} = 1.733 \pm 0.071$		10^{12} dyn/cm^2
	$C_{13} = 1.362 \pm 0.081$		10^{12} dyn/cm^2
	$C_{33} = 4.699 \pm 0.081$		10^{12} dyn/cm^2
	$C_{44} = 1.239 \pm 0.007$		10^{12} dyn/cm^2
	$C_{66} = 1.886 \pm 0.050$		10^{12} dyn/cm^2
Dielectric constants[c,d]	a axis	c axis	
	$\epsilon_0 = 86$	170	dimensionless
	$\epsilon_\infty = 6.843$	8.427	dimensionless
Scattering lengths[e]	$b_{Ti} = -0.34$		10^{-12} cm
	$b_O = 0.577$		10^{-12} cm
Neutron cross sections[e]	Ti	O	
$\sigma_{coherent}$	1.45	4.2	10^{-24} cm^2
$\sigma_{incoherent}$	2.95	0.04	10^{-24} cm^2
$\sigma_{absorption}$	3.5	0.0001	10^{-24} cm^2

[a]M. E. Straumanis, T. Ejima, and W. J. James, Acta Cryst. 14, 493 (1961). See also, W. H. Baur, Acta Cryst. 9, 515 (1956), and D. T. Cromer and K. Herrington, J. Am. Chem. Soc. 77, 4708 (1955).

[b]See Ref. 8.

[c]See Ref. 10.

[d]$\epsilon_\infty = n^2$ using the indices of refraction of D. C. Cronemeyer, in MIT Laboratory for Insulation Research Report No. 46, 1951 (unpublished).

[e]G. E. Bacon, *Neutron Diffraction*, 2nd ed. (Oxford U. P., London, 1962), pp. 31 and 61.

where $\Phi_{\alpha\beta}(0\kappa, l'\kappa')$ is the force constant describing the αth component of force on atom (0κ) due to a displacement of atom $(l'\kappa')$ in the β direction; $\vec{q} = 2\pi/\lambda$ is the wave vector of the phonon disturbance, and $\vec{r}(l\kappa)$ is the vector position of the κth atom in unit cell l. The $\underline{\Phi}$ matrices are of the form

$$\underline{\Phi}(0\kappa, l'\kappa') = \begin{pmatrix} \phi_{xx} & \phi_{xy} & \phi_{xz} \\ \phi_{yx} & \phi_{yy} & \phi_{yz} \\ \phi_{zx} & \phi_{zy} & \phi_{zz} \end{pmatrix} . \qquad (3)$$

However, the symmetry of the crystal may require some of the $\phi_{\alpha\beta}$ to be interdependent. Also, by assuming that the interatomic forces are central forces, one may describe the tensor force constants $\phi_{\alpha\beta}$ in terms of two force constants ϕ_r and ϕ_t, where $\phi_r = \partial^2\phi/\partial r^2$ is the bond-stretching or radial force constant and $\phi_t = (1/r)(\partial\phi/\partial r)$ is the bond-bending or tangential force constant. In this work we apply both central and tensor force models. However, the oxygen-oxygen [3]-[4] interaction (see Fig. 1 for labeling of atom positions) is constrained to be central throughout this work, since in tensor form that interaction contributes an excessive number of parameters to the models. The force constant matrices are given in Table II. The particular bond system used was chosen by considering the ionic separation distances. The interactions were terminated at second neighbors to limit the number of disposable parameters.

It is well known[18,19] that the $\underline{R}$ and $\underline{Z}\underline{C}\underline{Z}$ matrices must satisfy the translational invariance condition; that is, if the crystal is bodily moved (every atom is given the same displacement), the sum of the forces must be zero since no internal distortion has taken place between any atom pair. The result of applying the translational invariance con-

TABLE II. Force constant matrices used in the analysis of rutile data.

Atom pair $\kappa\kappa'$	Position of κ'	ϕ Matrix
11	(0, 0, c)	$P(1)$ $P(2)$ 0 $P(2)$ $P(1)$ 0 0 0 $P(3)$
13	(u, u, 0)	$P(4)$ $P(5)$ 0 $P(5)$ $P(4)$ 0 0 0 $P(6)$
23	(u, u, 1)	$P(7)$ $P(8)$ $P(9)$ $P(8)$ $P(7)$ $P(9)$ $P(10)$ $P(10)$ $P(11)$
35	($1-u$, $1-u$, 0)	$P(14)$ $P(15)$ 0 $P(15)$ $P(14)$ 0 0 0 $P(16)$
34	($\frac{1}{2}+u$, $\frac{1}{2}-u$, $\frac{1}{2}$)	$\phi_{xy} = \dfrac{r_x(34)\, r_y(34)}{[r(34)]^2} \times (\phi_r - \phi_t) + \phi_t \delta_{xy}$

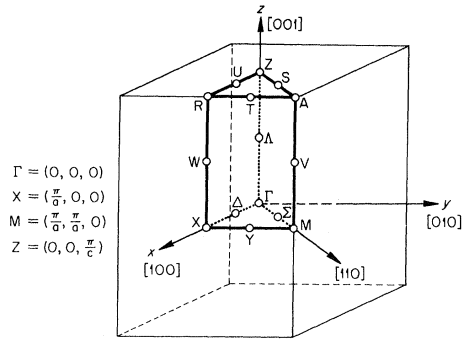

FIG. 2. Brillouin zone for the primitive tetragonal lattice. Labeling is in the notation of Koster (see Ref. 27).

dition to the $\underline{R}$ matrix is, for example, that the self-term force constant is defined as

$$\Phi_{\alpha\beta}(0\kappa, 0\kappa) = -\sum_{l',\kappa}{}' \Phi_{\alpha\beta}(0\kappa, l'\kappa') , \tag{4}$$

where the prime on the summation indicates that the $l' = 0$, $\kappa' = \kappa$ term is omitted.

B. Shell Model

Because the rigid-ion model has no means of accounting for the polarizability of the ions, several workers[20–22] suggested that the ion be considered as an inner core (positively charged) and an outer valence electron shell, which may be displaced relative to the core. This shell model has been discussed at length for cubic structures with most workers following the approach of Woods *et al.*,[22] Cowley *et al.*,[23] and Cochran *et al.*[24]

To extend the model to the tetragonal structure, we followed the original approach of Woods *et al.* in writing a $6n \times 6n$ (n is the number of atoms in the primitive cell) equation of motion in the displacements of the cores and, independently, the shells. Imposing the translational invariance condition on that $6n \times 6n$ equation, we find a general result slightly different in form from that of Woods *et al.* or Cochran *et al.* The matrix equation may be written in the form

$$\begin{aligned} \underline{M}\omega^2 \underline{U} &= (\underline{R} + \underline{Z}\underline{C}\underline{Z})\,\underline{U} + (\underline{T} + \underline{Z}\underline{C}\underline{Y})\,\underline{W}, \\ \underline{0} &= (\underline{T}^{\dagger} + \underline{Y}\underline{C}\underline{Z})\,\underline{U} + (\underline{\zeta} + \underline{Y}\underline{C}\underline{Y})\,\underline{W}, \end{aligned} \tag{5}$$

where the $\underline{T}$ matrix describes the interaction of an ion with the shell of its neighbor, $\underline{Y}$ is a diagonal matrix of shell charges, and $\underline{W}$ is a matrix of column vectors which are defined such that $\underline{Y}\underline{W}$ gives the dipole moments of the ions. The shell mass is taken as zero. The $\underline{\zeta}$ matrix is given by

$$\begin{aligned} \zeta^{\kappa\kappa'}_{\alpha\beta}(\vec{q}) = S^{\kappa\kappa'}_{\alpha\beta}(\vec{q}) + \delta_{\kappa\kappa'}\{k_\kappa\delta_{\alpha\beta} + T^{\kappa\kappa}_{\alpha\beta}(\vec{q}=0) \\ - S^{\kappa\kappa}_{\alpha\beta}(\vec{q}=0) + [\underline{Y}\underline{C}(\vec{q}=0)\,\underline{Z}]^{\kappa\kappa}_{\alpha\beta}\} , \end{aligned} \tag{6}$$

where the $\underline{S}$ matrix describes the shell-shell interactions, k_κ is the force constant between the core and shell of ion κ, and the $[\underline{Y}\underline{C}(\vec{q}=0)\,\underline{Z}]^{\kappa\kappa}_{\alpha\beta}$ is the Coulomb self-term from the $\underline{Y}\underline{C}\underline{Z}$ matrix. It is this expression which differs from the similar definition by Cochran *et al.* (their results are not affected); they require $\beta = \alpha$ in the T and S terms in the braces, saying that the core-shell interaction $\underline{F} = \underline{T} - \underline{S}$ is diagonal. The $\underline{F}$ interaction may not be diagonal for noncubic structures, and $\underline{\zeta}$ has been generalized. Cochran's equation does not include the $\underline{Y}\underline{C}\underline{Z}$ term, which is zero for the cubic symmetry discussed in their paper, but which is not zero for rutile.

In this work we have used the simple shell model, which assumes that the short-range forces are of shell-shell type only, by setting $\underline{T} = \underline{S} = \underline{R}$. We, along with others,[23,25] have attempted to include some core-shell interaction by setting $\underline{S} = \gamma\underline{R}$, only to find that allowing γ to be significantly different from unity made no noticeable change in the agreement between the calculated and measured dispersion curves. Thus, γ is set equal to unity throughout the remainder of this paper.

C. Factorization of Dynamical Matrix

The dynamical matrices for rutile are 18×18 complex matrices. However, along the principal symmetry directions of the Brillouin zone, the 18×18 matrix may be factorized into block matrices.[26–28] The Brillouin zone for rutile is shown in Fig. 2, and the symmetry decompositions for the principal symmetry directions are given in Table III, where the superscripts preceding the Koster symbol give the degeneracy of the irreducible representation. As an example of the notation to be used in the remainder of this work, the symbol $^1\Sigma_2(3)$ represents a phonon of the third lowest branch of the Σ_2 representation, which is singly degenerate.

Following Dayal,[12] we give the symmetry of the optic modes at zero wave vector in Fig. 3. The Γ_1^+, Γ_2^+, Γ_3^+, Γ_4^+, and Γ_5^- modes have oxygen-only

TABLE III. Irreducible representations for selected points in Brillouin zone for rutile structure.

Point in Brillouin zone	$\vec{q}$	Irreducible representations
Γ	$(0,0,0)$	$^1\Gamma_1^+ + {}^1\Gamma_2^+ + {}^1\Gamma_3^+ + {}^1\Gamma_4^+ + 4\,{}^2\Gamma_5^+ + 2\,{}^1\Gamma_1^- + 2\,{}^1\Gamma_4^- + {}^2\Gamma_5^-$
Δ	$(\zeta,0,0)$	$6\,{}^1\Delta_1 + 3\,{}^1\Delta_2 + 6\,{}^1\Delta_3 + 3\,{}^1\Delta_4$
Σ	$(\zeta,\zeta,0)$	$6\,{}^1\Sigma_1 + 5\,{}^1\Sigma_2 + 6\,{}^1\Sigma_3 + {}^1\Sigma_4$
Λ	$(0,0,\zeta)$	$3\,{}^1\Lambda_1 + {}^1\Lambda_2 + {}^1\Lambda_3 + 3\,{}^1\Lambda_4 + 5\,{}^2\Lambda_5$
χ	$(\pi/a,0,0)$	$6\,{}^2\chi_1 + 3\,{}^2\chi_2$
M	$(\pi/a,\pi/a,0)$	$^2M_{1,2} + {}^2M_{3,4} + 2\,{}^2M_{5,6} + 4\,{}^2M_9^+ + {}^2M_9^-$
Z	$(0,0,\pi/c)$	$3\,{}^2Z_1 + 2\,{}^2Z_2 + {}^2Z_3 + 3\,{}^2Z_4$

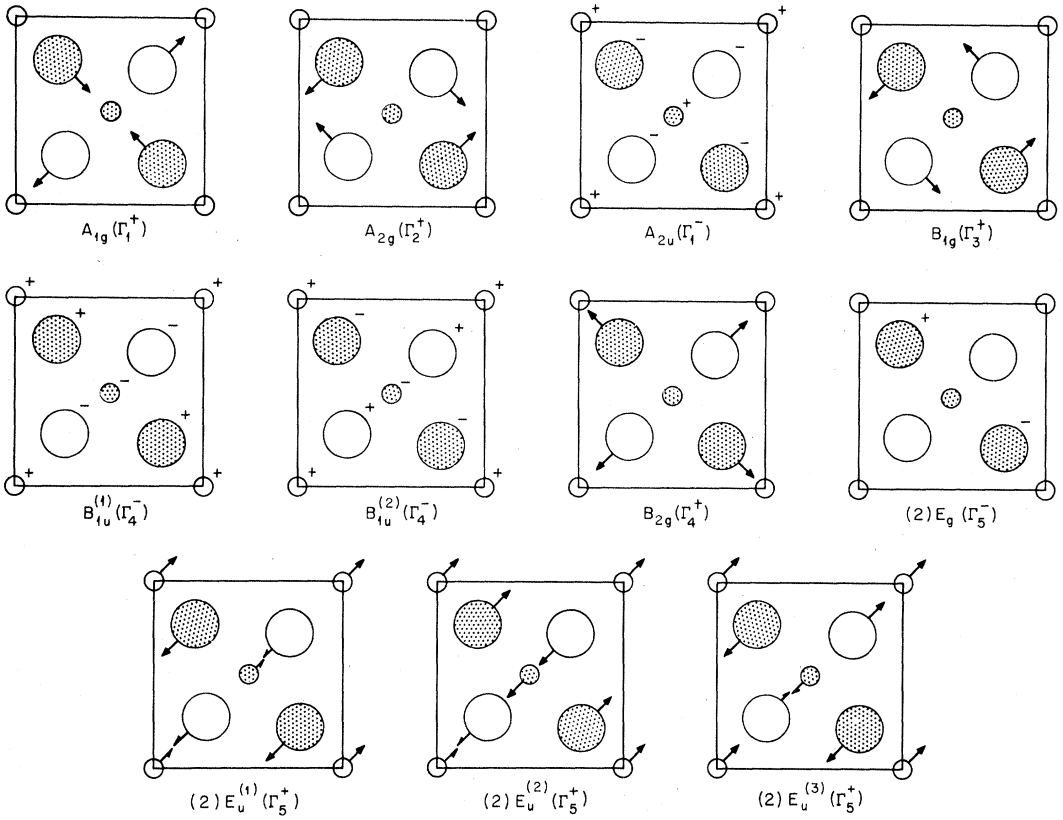

FIG. 3. Symmetry of the optic modes of the rutile structure for zero wave vector. Labeling is in the notation of Mulliken and, in parentheses, of Koster. Doubly degenerate modes are indicated by a "(2)" preceding the Mulliken symbol.

displacements. Furthermore, for the first four of these modes, oxygens [3] and [5] are moving in directions normal to the displacements of oxygens [4] and [6], and it is not possible to label these modes as transverse or longitudinal for wave vectors in the $xy0$ plane. There is motion of the titanium atoms for the Γ_1^- and Γ_4^- modes in which the displacements are along the z axis and for the Γ_5^+ modes with displacements in the $xy0$ plane.

Consider the Γ_5-type modes. The symmetry of the space group D_{4h}^{14} requires that the Γ_5 modes be doubly degenerate. For each of the Γ_5^+ modes in Fig. 3, there is a similar mode which has displacement vectors rotated by $\frac{1}{2}\pi$ from them. For phonon wave vectors along [110], a pair of these modes would comprise LO and TO modes. From the space-group symmetry alone, the modes would be degenerate since the atomic environment is the same for both. However, the long-range Coulomb field of the crystal may split the degeneracy of polar modes in which an electric dipole moment is created in the unit cell. For rutile, which is tetragonal, the splitting is dependent on the direction of approach[7] to $\vec{q}=0$. That is, for wave vectors in the $xy0$ plane $[\vec{q}=(q_x, q_y, 0)]$, the doubly degenerate Γ_5^+ modes are split into distinct TO and LO modes. These degeneracies are *not* split for wave vectors approaching $\vec{q}=0$ along the c axis, since both the Γ_5^+ with [110] displacements and the Γ_5^+ with $[1\bar{1}0]$ displacements are *transverse* to the direction of propagation of the phonons. Thus, both vibrations experience the same transverse Coulomb field, and they are not split in energy. (The TO frequency one measures with wave vectors approaching $\vec{q}=0$ along the c axis is identical to the TO frequency measured with wave vectors approaching $\vec{q}=0$ in the $xy0$ plane.)

The Γ_5^- degeneracy at $\vec{q}=0$ is not dependent upon the direction of approach to $\vec{q}=0$. The two Γ_5^- modes are not polar modes; one has oxygens [4] and [6] moving as shown in Fig. 3, with [3] and [5] fixed, while the other mode has [3] and [5] vibrating out of phase along the z axis with [4] and [6] fixed. Both modes experience the same short-range force field, and the degeneracy is not split.

The Γ_1^- mode is the only polar mode with c axis displacements. It is measured as a TO mode for $\vec{q}\to 0$ in the $xy0$ plane and as an LO mode for $\vec{q}\to 0$ along the z axis. The polar state created in the crystal by this mode has all titanium ions (positive) displaced oppositely to the oxygen (negative) ions, similar to a possible ferroelectric state of the crys-

tal which is discussed in Sec. IID.

D. Relation of Polar Modes and Dielectric Constants

Cochran[29] generalized the Lyddane-Sach-Teller relation for cubic crystals with more than two atoms per unit cell:

$$\frac{\epsilon_0}{\epsilon_\infty} = \prod_i \frac{[\nu_i^2(\vec{q}\to 0)]_i}{[\nu_t^2(\vec{q}\to 0)]_i}, \tag{7}$$

where ϵ_0 $\{\epsilon_\infty\}$ is the static {high-frequency} dielectric constant and $[\nu_i^2(\vec{q}\to 0)]_i$ $\{[\nu_t^2(\vec{q}\to 0)]_i\}$ is the square of the ith longitudinal {tranverse} optic-phonon-mode frequency at zero wave vector. Barker[30] showed that for a uniaxial crystal, the expression may be separated; if c is the unique axis and a is normal to c, then

$$\frac{\epsilon_{c,0}}{\epsilon_{c,\infty}} = \prod_i \frac{[\nu_{c,l}^2(\vec{q}\to 0)]_i}{[\nu_{c,t}^2(\vec{q}\to 0)]_i}, \tag{8}$$

and there is a similar expression for the a axis. For rutile, there is only one pair of LO-TO polar modes with displacements along the c axis, namely, the Γ_1^- modes, and Eq. (8) becomes

$$\frac{\epsilon_{c,0}}{\epsilon_{c,\infty}} = \frac{[\nu_{c,l}^2(\vec{q}\to 0)]_{\Gamma_1^-}}{[\nu_{c,t}^2(\vec{q}\to 0)]_{\Gamma_1^-}} . \tag{9}$$

Cochran[11] related dielectric constants to soft phonon modes for ferroelectric materials with the relations

$$\epsilon_0(T) \sim 1/(T - T_C) , \tag{10}$$

$$\nu_i^2(T) \sim (T - T_C) , \tag{11}$$

where T_C is the Curie temperature of the ferroelectric transition. The temperature dependence of the frequency of the Γ_1^- mode is investigated in this paper.

III. EXPERIMENT

The experimental methods of using coherent inelastic scattering of thermal neutrons to measure phonon dispersion curves are now well known. Neutrons of energy $E_0 = \hbar^2 k_0^2/2m_n$ and momentum $\hbar\vec{k}_0$ are incident on the sample, and are scattered with energy $E' = \hbar^2 k'^2/2m_n$ and momentum $\hbar\vec{k}'$ if the conservation conditions

$$\vec{k}_0 - \vec{k}' = \vec{Q} = 2\pi\vec{\tau} - \vec{q} , \tag{12}$$

$$E_0 - E' = \pm h\nu , \tag{13}$$

are satisfied. The + (−) signs refer to phonon creation (annihilation), $\vec{q}$ is the wave vector, and $h\nu$ is the energy of the phonon; $\vec{\tau}$ is a reciprocal lattice vector.

The present measurements were made at the Oak Ridge National Laboratory (ORNL) High Flux Isotope Reactor with the computer-controlled HB-3 triple-axis spectrometer facility.[31] The large majority of the measurements were made with the "constant $\vec{Q}$" method,[32] although "constant E" scans and scans in which both E and $\vec{Q}$ were varied were employed when necessary. Most of the data were collected using the (101) plane of beryllium as the monochromator and the (111) plane of germanium as the analyzer, with 2/3 degree slits before and after the sample. The low-temperature experiments were performed with the sample sealed in a helium gas atmosphere inside an aluminum can which was mounted inside a liquid-helium cryostat. A resistance heater was positioned between the sample and the liquid-helium bath, and copper-

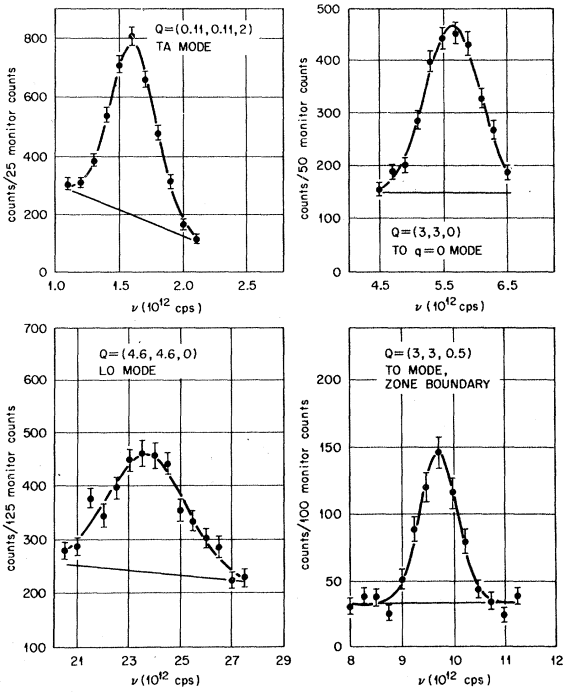

FIG. 4. Neutron intensity scans for various phonons showing the fitted Gaussian functions.

TABLE IV. Rutile specimens used in experiment.

Full-width at half-maximum of rocking curve (deg)	Volume (cm^3)	Orientation of Boule axis	Source
0.24	4.0	[001]	On loan from G. W. Clark, ORNL (Linde grown)
0.28	11.0	[001]	On loan from R. A. Weeks, ORNL (Linde grown)
0.42	19.2	[110]	Purchased from National Lead Co., Titanium Division (M. D. Beals, grower).

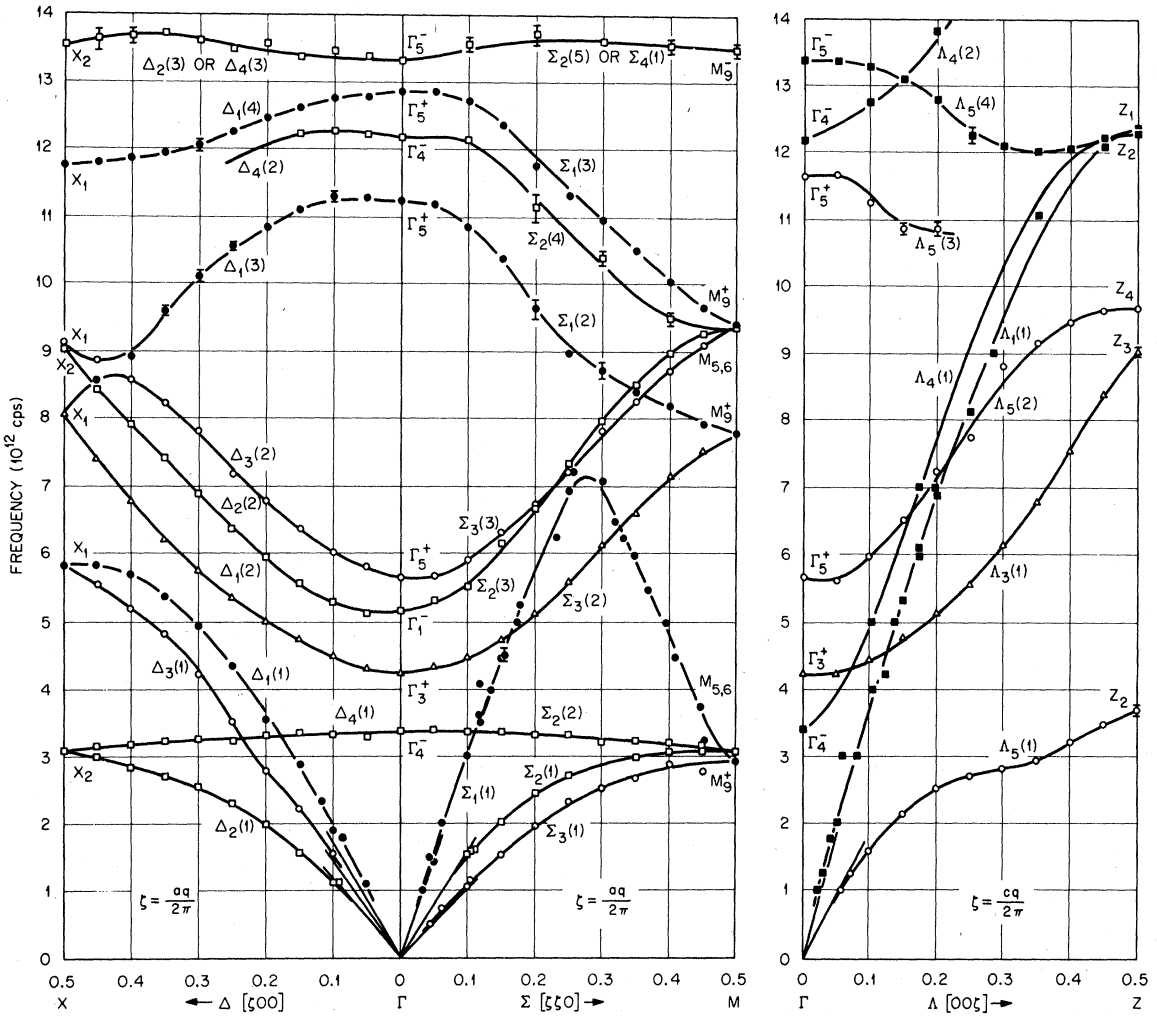

FIG. 5. Phonon dispersion relation of rutile as determined by coherent inelastic neutron scattering (low-frequency data). Lines through the data points are guide lines only.

constantan thermocouples were installed at opposite ends of the sample. Three samples were used in the investigation (see Table IV). The results from the three crystals were consistent.

Each of the approximately 950 neutron peaks observed in the experiment was fitted to Gaussian functions by a nonlinear least-squares-fitting routine which allowed two Gaussians, one Lorentzian, and a cubic polynomial background function to be fitted. In most cases a single Gaussian and a linear sloping background provided adequate fits, as shown in Fig. 4.

IV. RESULTS AND CALCULATIONS

A. Data

The measured phonon dispersion relations for phonons propagating along the [100], [110], and [001] directions are shown in Fig. 5 (low-frequency data) and Fig. 6 (high-frequency data). The branches are labeled in the notation of Koster, following the paper by Gay *et al.*[27] The experimental errors are believed to be of the order of 1%; if a particular data point has an error larger than the plotted point, an error bar is indicated. The straight solid lines near $\nu \to 0$, $\vec{q} \to 0$ represent the acoustic-phonon branch slopes as calculated from the measured elastic constants.[8] The solid (open) points represent measurements made under predominately longitudinal (transverse) scattering conditions. The circular (square) points indicate that the scattering vector $\vec{Q}$ lay predominately normal to (parallel to) the z axis. The triangular points represent modes with displacements normal to z, but which may not be classified as longitudinal or transverse.

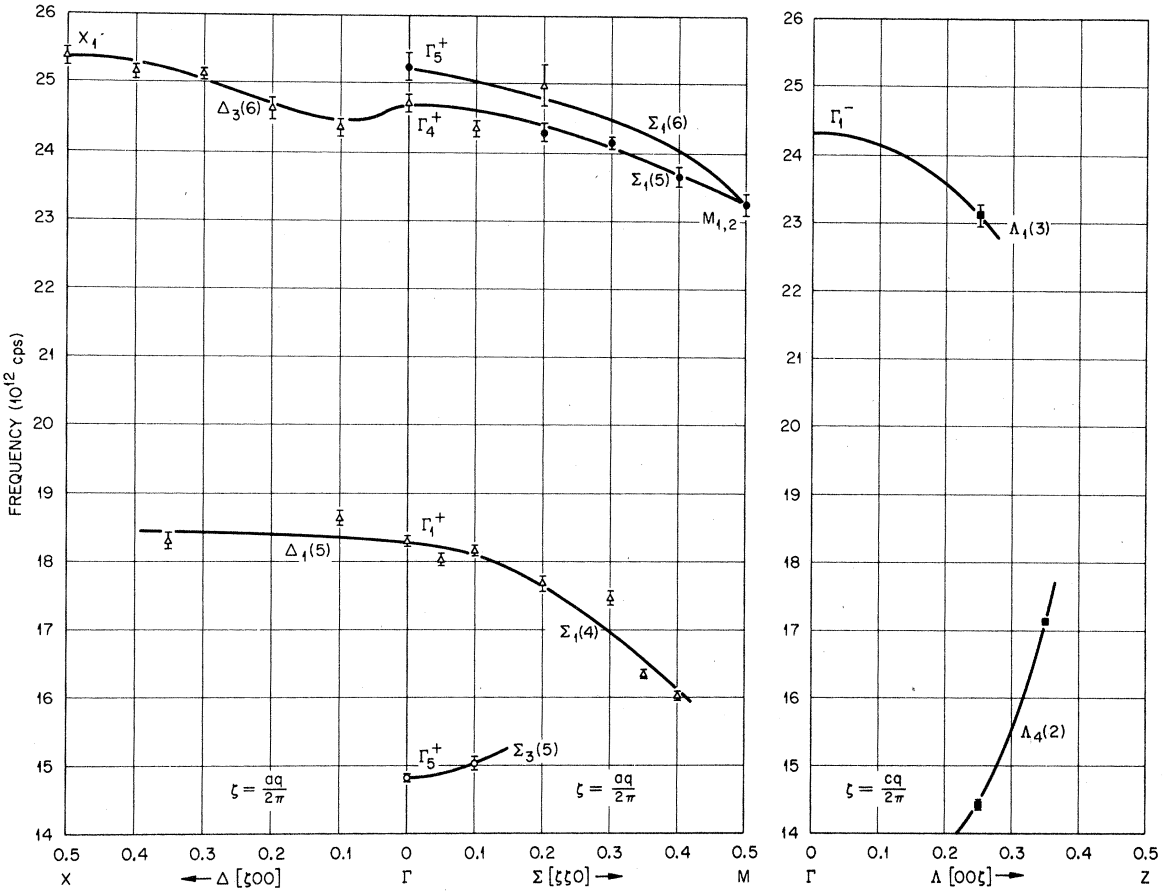

FIG. 6. Phonon dispersion relation of rutile as determined by coherent inelastic neutron scattering (high-frequency data). Lines through the data points are guide lines only.

Values of the phonon frequencies at the Γ, *X*, *M*, and *Z* points are given in Table V. (Complete tabulations of the measured data are available by request from the authors.) The errors given in Table V represent the larger of (i) the statistical error as determined by the peak-fitting program or (ii) 1% of the measured frequency. Where more than one determination of a phonon frequency has been made, the statistical average of the determinations is given.

It is seen from Fig. 5 that the measured acoustic branches have slopes in good agreement with the slopes predicted by the elastic constant measurements, except for the LA branches in the [100] and [001] directions. The differences in the two LA branches are larger than the errors in the measurements and are thought to be real.

B. Calculations from Models

Various forms of the rigid-ion and shell models were fitted to the measured dispersion relations by nonlinear least-squares methods with the force constants as variables (see Table VI). In order to be acceptable, each model was required to satisfy two criteria: (i) All calculated frequencies had to be real. (ii) All zone boundary degeneracies had to agree with those observed experimentally. It was found that all eight models could be forced to satisfy criterion (i). However, imposing criterion (ii) on the resulting models eliminated all except models VII and VIII, the shell models with tensor forces.

The failure of the models to satisfy the zone boundary degeneracies observed experimentally stems from the symmetry requirement that no two branches belonging to the same irreducible representation can become degenerate; that is, the branches cannot cross one another in $(\vec{q}, \nu)$ space. Suppose it is found experimentally that $\Sigma_1(2) \rightarrow \Sigma_3(2)$ at the zone boundary, and $\Sigma_1(3) \rightarrow \Sigma_3(3)$. (These modes are uniquely defined by their eigenvectors.) If a model calculates the mode identified experimentally as $\Sigma_1(2)$ to be higher in frequency than the $\Sigma_1(3)$ mode, then the model must necessarily predict that $\Sigma_1(2) \rightarrow \Sigma_3(3)$ and $\Sigma_1(3) \rightarrow \Sigma_3(2)$ at the zone boundary. This result disagrees with the experiment, and the model is rejected. None of the models using axially symmetric forces was able to satisfy

TABLE V. Phonon frequencies in rutile at high-symmetry points of Brillouin zone.

Koster notation[a]	Mulliken notation	Optical determination[b] (10^{12} cps)	Neutron determination[c] (10^{12} cps)	Corresponding X-point determination[c] (10^{12} cps)	Corresponding M-point determination[c] (10^{12} cps)	Corresponding Z-point determination[c] (10^{12} cps)
Optic modes:						
Γ_4^+	B_{2g}	R: 24.78	24.72 ± 0.25	X_1: 25.38 ± 0.25	$M_{1,2}$: 23.26 ± 0.23	NF
Γ_5^+	E_u (LO)	I: 24.18	25.24 ± 0.34	X_1: 24.38 ± 0.25	$M_{1,2}$: 23.26 ± 0.23	does not apply[d]
Γ_1^-	A_{2u} (LO)[e]	I: 24.33	NF	does not apply	Does not apply	NF
Γ_2^+	A_{2g}	NA	NF	NF	NF	NF
Γ_1^+	A_{1g}	R: 18.36	18.30 ± 0.46	NF	NF	NF
Γ_5^+	E_u (TO)	I: 15.00	14.81 ± 0.15	NF	NF	NF
Γ_5^-	E_g	R: 13.41	13.339 ± 0.181	X_2: 13.528 ± 0.135	M_9^+: 13.522 ± 0.135	Z_2: 12.312 ± 0.123
Γ_5^+	E_u (LO)	I: 13.74	12.853 ± 0.129	X_1: 11.756 ± 0.118	M_9^+: 9.442 ± 0.094	Does not apply[d]
Γ_4^-	B_{1u}^2	NA	12.182 ± 0.122	X_2: 9.033 ± 0.09	$M_{5,6}$: 9.398 ± 0.094	NF
Γ_5^+	E_u (TO)	I: 11.64	NF	NF	NF	NF
Γ_5^+	E_u (LO)	I: 11.19	11.232 ± 0.112	X_1: 9.130 ± 0.125	M_9^+: 7.811 ± 0.078	Does not apply[d]
Γ_5^+	E_u (TO)	I: 5.49	5.661 ± 0.075	X_1: 8.071 ± 0.081	M_9^+: 9.442 ± 0.133	Z_4: 9.720 ± 0.097[d]
Γ_1^-	A_{2u} (TO)[e]	I: 5.01	5.177 ± 0.052	X_2: 9.033 ± 0.090	$M_{5,6}$: 9.398 ± 0.094	Does not apply[e]
Γ_3^+	B_{1g}	R: 4.29	4.246 ± 0.094	X_1: 8.071 ± 0.081	M_9^+: 7.811 ± 0.078	Z_3: 9.040 ± 0.090
Γ_4^-	B_{1u}	NA	3.389 ± 0.057	X_2: 3.084 ± 0.031	$M_{5,6}$: 3.058 ± 0.056	Z_1: 12.397 ± 0.124
Acoustic modes:						
Γ_5^+	E_u	NA	0.0	X_1: 5.821 ± 0.058 (LA)	M_9^+: 2.936 ± 0.070 (LA)	Does not apply[d]
Γ_5^+	E_u	NA	0.0	X_1: 5.821 ± 0.058 (TA)	M_9^+: 2.936 ± 0.070 (TA)	Z_2: 3.697 ± 0.069[d] (TA)
Γ_1^-	A_{2u}	NA	0.0	X_2: 3.084 ± 0.031 (TA)	$M_{5,6}$: 3.058 ± 0.056 (TA)	Z_1: 12.397 ± 0.124 (LA)

[a]See J. G. Gay, W. A. Albers, Jr., and F. J. Arlinghaus, J. Phys. Chem. Solids 29, 1449 (1968).

[b]Raman data (R) from S. P. S. Porto, P. A. Fleury, and T. C. Damen, Phys. Rev. 154, 522 (1967), and infrared data (I) from D. M. Eagles, J. Phys. Chem. Solids 25, 1243 (1964) (NA = not active).

[c]NF = not found.

[d]Each Γ_5^+ mode is doubly degenerate along $\Gamma\Lambda Z$.

[e]Γ_1^- mode is TO along $\Gamma\Delta X$ and $\Gamma\Sigma M$, and is LO along $\Gamma\Lambda Z$.

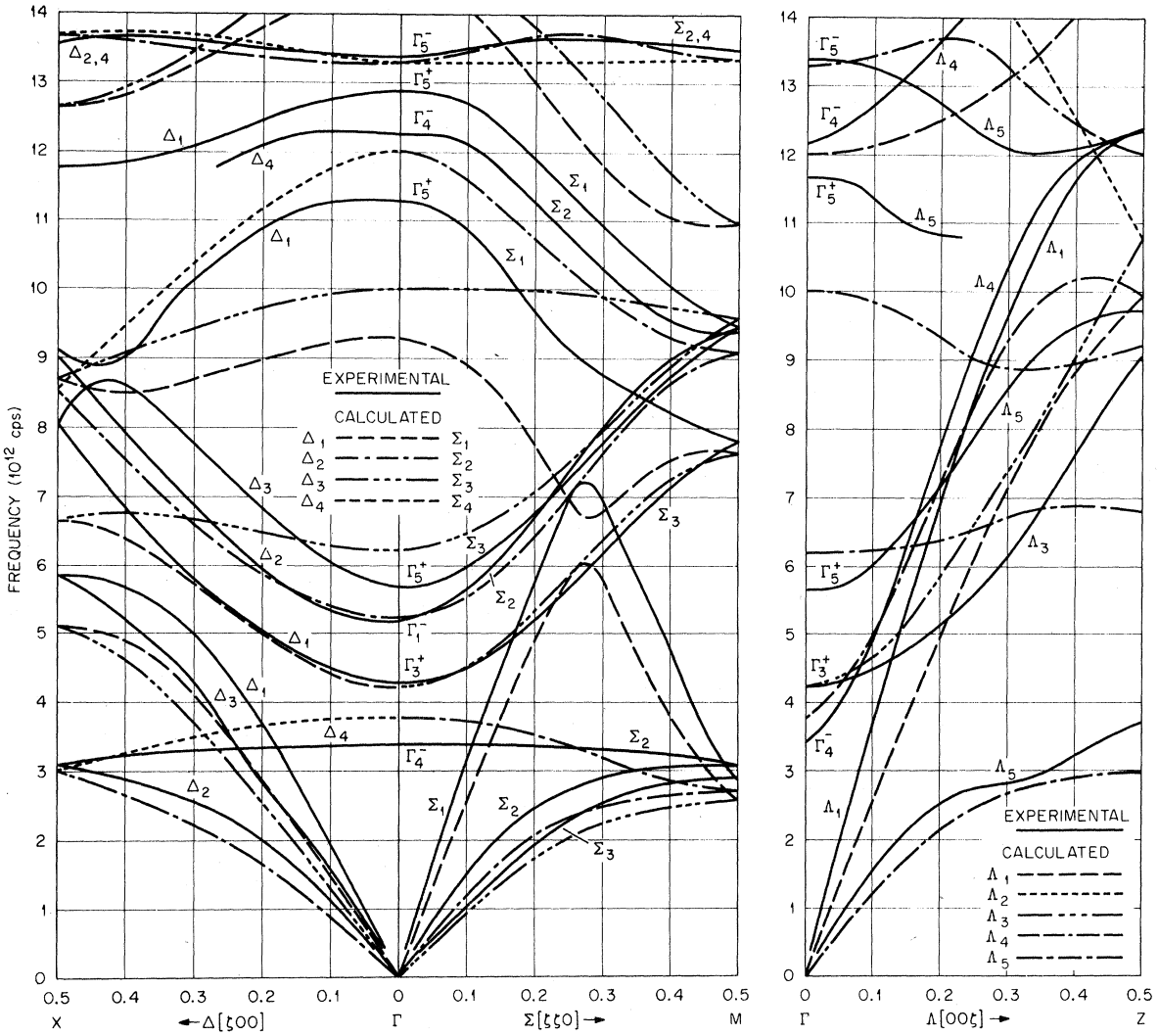

FIG. 7. Comparison of the dispersion relation calculated by RIM III with that measured in the neutron experiment (low frequencies). Solid lines are the measured curves and are labeled according to the irreducible representation of the branch.

criteria (i) and (ii) simultaneously.

Although only the shell models with tensor forces proved acceptable, both the rigid-ion model III and the shell model VII are presented in Figs. 7–9. (The rigid-ion model with axially symmetric forces is employed extensively in the literature. The rigid-ion model with tensor forces is presented here for the purposes of comparison.) Neither of the models presented includes Ti-Ti forces, since it was found that the Ti-Ti interaction had little effect on the calculations. In the figures the solid lines represent the measured curves, and the irreducible representation of each is given. The calculated curves are presented as dashed or dotted lines, where the symbols used indicate the irreducible representation of the branch.

The qualitative features of the data and the results of the calculations are discussed simultaneously, with the rigid-ion and shell models being referred to as RIM and SM, respectively. (It may prove helpful to refer to the diagram of the eigenvectors of each mode at $\vec{q}=0$, Fig. 3.) Notable features are the following:

(a) The RIM predicts the $\Sigma_3(3)$ and $\Sigma_3(4)$ branches become degenerate at the zone boundary. This calculation disagrees with the experimental degeneracy of $\Sigma_3(3) \rightarrow \Sigma_1(3)$. Another pair of incorrect degeneracies given by the RIM is $\Sigma_3(5) \rightarrow \Sigma_1(3)$. The SM predicts all degeneracies in accord with the measurements.

(b) The $\Sigma_1(1)$ LA branch interacts with the $\Sigma_1(2)$ branch which originates as Γ_5^+, $\nu = 11.23 \times 10^{12}$ cps. The sharply peaked appearance of the LA branch is given by both models. However, both models

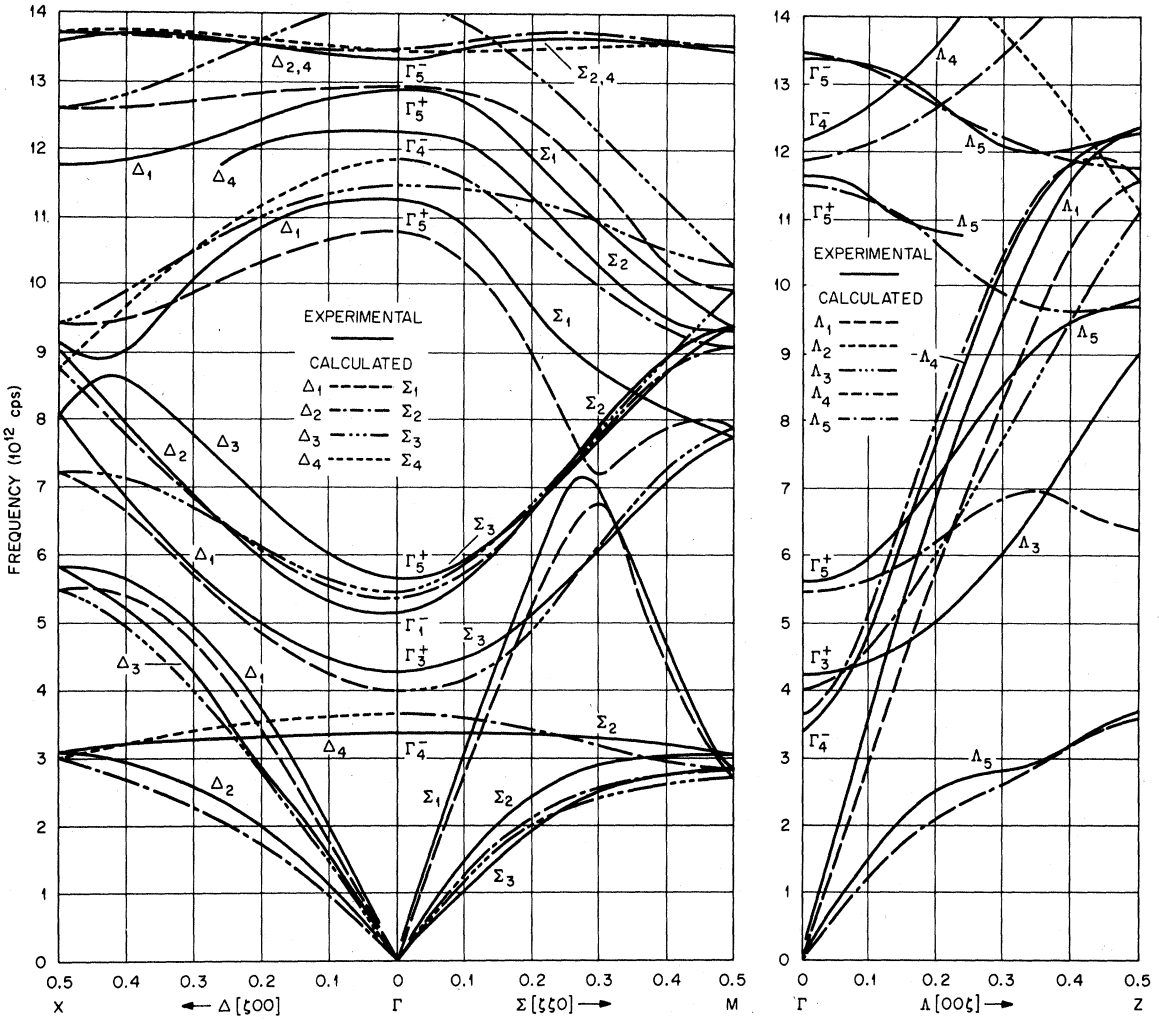

FIG. 8. Comparison of the dispersion relation calculated by SM VII and that measured in the neutron experiment (low frequencies). Solid lines are the measured curves and are labeled according to the irreducible representation of the branch.

predict a sharp dip in the $\Sigma_1(2)$ branch; no such dip of $\Sigma_1(2)$ was seen experimentally.

(c) The Λ_5 TA mode has a definite dip at $\vec{q} \simeq (0, 0, 0.33)$. The SM calculation indicates similar structure at a wave vector slightly displaced from that of the measurement; the RIM calculation shows no indication of a dip.

(d) The Δ_3 TA branch also exhibits structure at $\vec{q} = (0.20, 0, 0)$; neither model demonstrates this feature.

(e) Both models are in serious disagreement with the $\Lambda_5(2)$ mode near the zone boundary.

The general features of the models may be seen by comparing calculations and measurements in terms of four categories of modes: acoustic modes, optic modes which create an electric dipole moment in the lattice at $\vec{q} = 0$ (polar modes), optic modes which cause each O-Ti-O unit to have a dipole moment at $\vec{q} = 0$, but, because of out-of-phase motion of adjacent O-Ti-O units, create no net dipole moment in any unit cell, and optic modes which create no dipole moments between ions.

(a) The acoustic modes are, in every case, fitted

TABLE VI. Models used to fit rutile phonon data.

Number	Ion structure	Force type	Included Ti-Ti forces
I	RIM	Axially summetric	No
II	RIM	Axially symmetric	Yes
III	RIM	Tensor[a]	No
IV	RIM	Tensor[a]	Yes
V	SM	Axially symmetric	No
VI	SM	Axially symmetric	Yes
VII	SM	Tensor[a]	No
VIII	SM	Tensor[a]	Yes

[a]Oxygen-Oxygen interaction out of the xy plane is constrained to be axially symmetric.

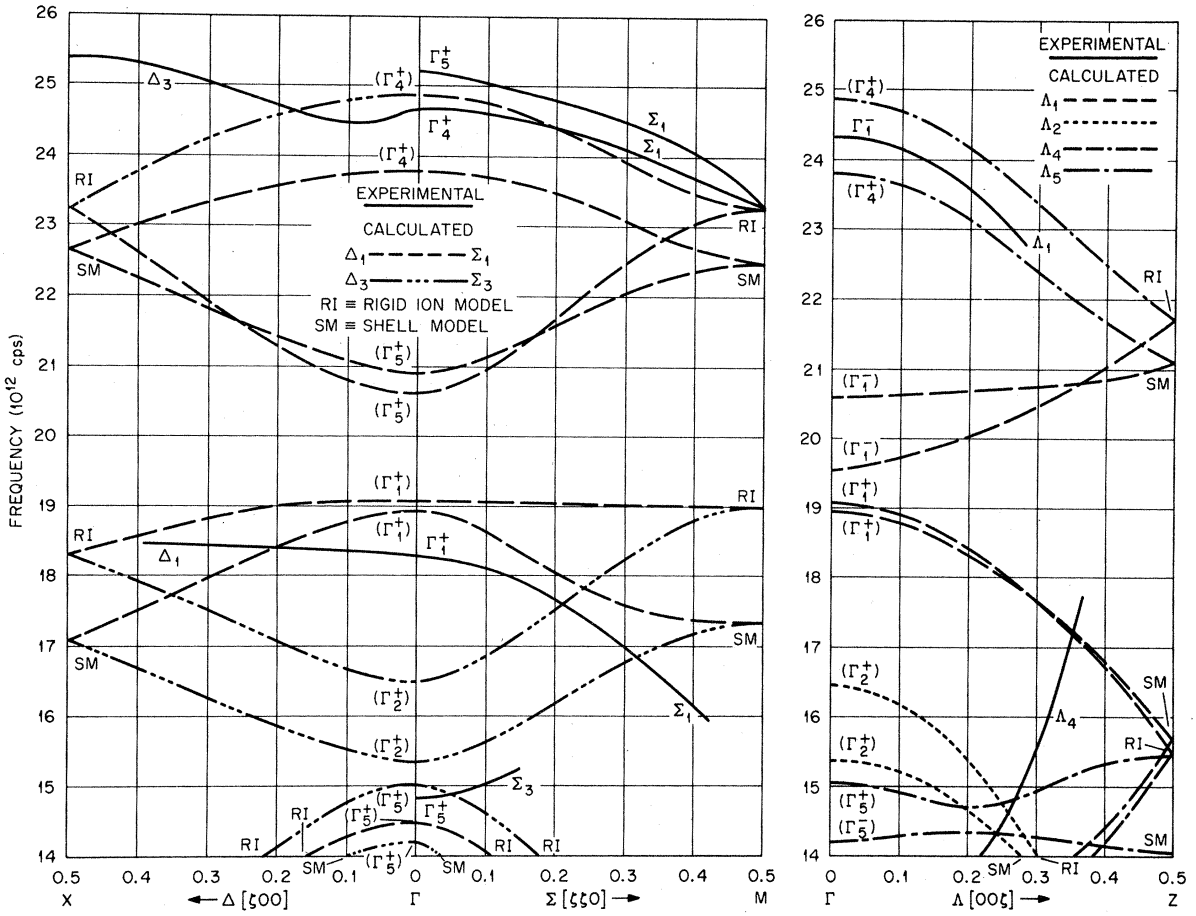

FIG. 9. Comparison of the dispersion relation calculated by both RIM III and SM VII with the measured curves at high frequencies. Solid lines are the measured curves.

better by the SM than the RIM. However, the zone boundary frequencies of all of the calculated acoustic modes of both models are lower than the measured frequencies.

(b) As is expected from the construction of the two models, the SM gives closer agreement with the measured frequencies of the polar modes. An extreme example is the $\Sigma_1(3)$ mode (Γ_5^+, $\nu = 12.85 \times 10^{12}$ cps) which is fitted reasonably well by the SM but very poorly by the RIM. (The frequency for $\vec{q} = 0$, as calculated by the RIM is approximately 13% too high.) Surprisingly, the RIM does fit some of the polar modes well. For example, the $\Sigma_2(3)$ mode (Γ_1^-, $\nu = 5.18 \times 10^{12}$ cps), the TO mode associated with the c-axis static dielectric constant, is fitted equally well by both models.

(c) The $\Sigma_4(1)$ mode (Γ_4^-, $\nu = 3.39 \times 10^{12}$ cps) is an example of a mode in which the O-Ti-O unit has an electric dipole moment at $\vec{q} = 0$, but the entire lattice does not. The SM again gives significantly better agreement with the experimental frequencies than does the RIM.

(d) The optic modes, in which no dipole moments between ions are created, still may produce *ionic* polarization owing to the physical distortion of the electron shells when the ion is displaced in the lat-

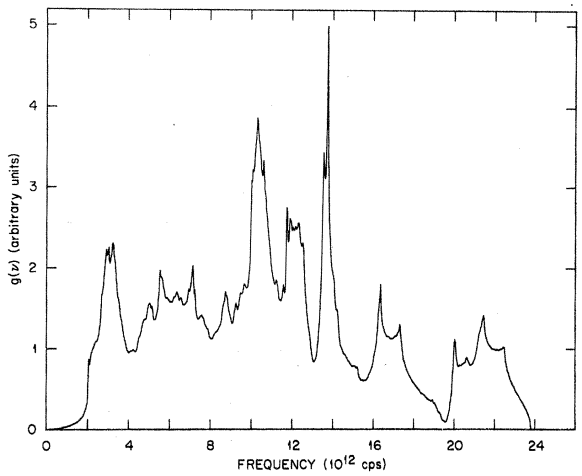

FIG. 10. Frequency distribution for SM VII calculated by the method of Ref. 33.

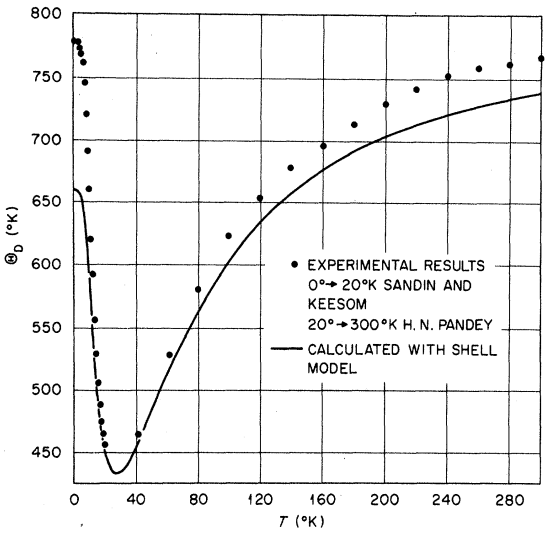

FIG. 11. Comparison of the Debye temperature for rutile as calculated from the frequency distribution for SM VII with the specific-heat measurements given in Refs. 35–38.

tice. Thus, one may expect the SM to give some small improvement over the RIM. The present result is that the RIM actually gives slightly better agreement with the experiment than the SM does.

The one-phonon density of states for the shell model VII has been calculated by the method of Gilat and Raubenheimer[33] as adapted by Mostoller[34] and is presented in Fig. 10. The distribution function has been used to calculate the specific heat and associated Debye temperature in the harmonic approximation as a function of temperature. The resulting Θ_D is shown in Fig. 11 along with the experimental values of Sandin and Keesom[35] (0.3 °K → 20 °K), and Dugdale *et al.*[36] and Shomate[37] (20 °K → 300 °K) as converted by Pandey.[38] That the room temperature model cannot predict the low-temperature Θ_D is not surprising because of the changes in the low-frequency optic modes with temperature (to be discussed in Sec. IV D).

C. Discussion of Best-Fit Parameters

During each iteration of the fitting procedure a standard error χ was calculated. Two separate tests were used to determine the end of a fitting cycle. The first test was comparison of χ for successive iterations; if $\chi(I+1) - \chi(I)$ were less than some predetermined convergence criterion, the model was considered to have converged. The second test involved the previously discussed unphysical degeneracies; if the model began to calculate unphysical degeneracies with succeeding iterations, the lowest-χ iteration having correct degeneracies was chosen as the best-fit limit of the model.

In the analysis of the present experiment, the fitting of RIM III was terminated by criterion (i) when the change in χ between successive iterations was less than 1%. The fitting of the SM VII was terminated by criterion (ii). For both models, large changes were being calculated for some parameters [namely, $P(9)$, $P(10)$, and $P(13)$] even in the final fitting step. Because of the possibility of correlations between these and the remaining parameters, it is felt that no parameter is known to an uncertainty less than 5%. The best-fit parameters and values for RIM III and SM VII are given in Table VII.

The similarities of the signs and the relative magnitudes of the parameters of the two models are obvious. These best-fit parameters offer additional indications of the necessity of using tensor forces to describe rutile; that is, if one assumes that the interatomic forces are central forces, certain interrelations among the tensor parameters are required, namely,

$$P(5) = P(4) - P(6), \quad P(9) = P(10),$$
$$P(15) = P(14) - P(16). \tag{14}$$

None of these relations is satisfied by the best-fit parameters of either of the models presented in Table VII. Note that the models predict the ratio of the effective charge to the ionic charge to be 0.55 (RIM) and 0.63 (SM). Fitting only $\vec{q} = 0$ data with RIM's, Katiyar and Krishnan[14] found 0.62. The best-fit values of the electronic polarizabilities in the SM are $\alpha(\mathrm{Ti}) = 0.36$ Å^3 and $\alpha(\mathrm{O}) = 0.48$ Å^3, which may be compared with the polarizabilities of Tessman, Kahn, and Shockley[39]: $\alpha(\mathrm{Ti}^{+4}) = 0.2$ Å^3 and $\alpha(\mathrm{O}^{-2}) = 0.9$ Å^3. [In Ref. 39 various values of

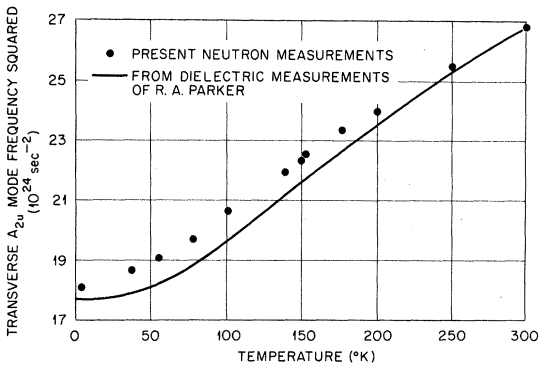

FIG. 12. Plot of the square of the frequency of the Γ_1^- (A_{2u}) mode as measured and as calculated from the static dielectric constant (c-axis) measurements of Parker (Ref. 10), as a function of temperature. The Lyddane-Sachs-Teller relation was used to calculate the TO frequency squared from $\epsilon_{c,o}$ by assuming that the product of the square of the LO frequency with the high-frequency dielectric constant was independent of temperature.

$\alpha(O^{-2})$ from 0.5 to 3.2 Å^3 are reported, as determined from different compounds. The value quoted here was calculated for oxygen atoms in SnO_2, which has the rutile structure.] The mechanical polarizabilities as determined by the shell model have the ratio $d(O)/d(Ti) = 4.2$.

D. Temperature Dependence of $\Gamma_1^-(A_{2u})$ Mode

The frequency of the $\Gamma_1^-(A_{2u})$ mode has been measured as a function of temperature from 4.2 to 300 °K. The two most striking features of the data are that the frequency observed at 300 °K decreases by 18% at 4.2 °K, and that at 300 °K the peaks in the phonon scans are symmetric and broad, while at low temperature the peaks are asymmetric and sharp.

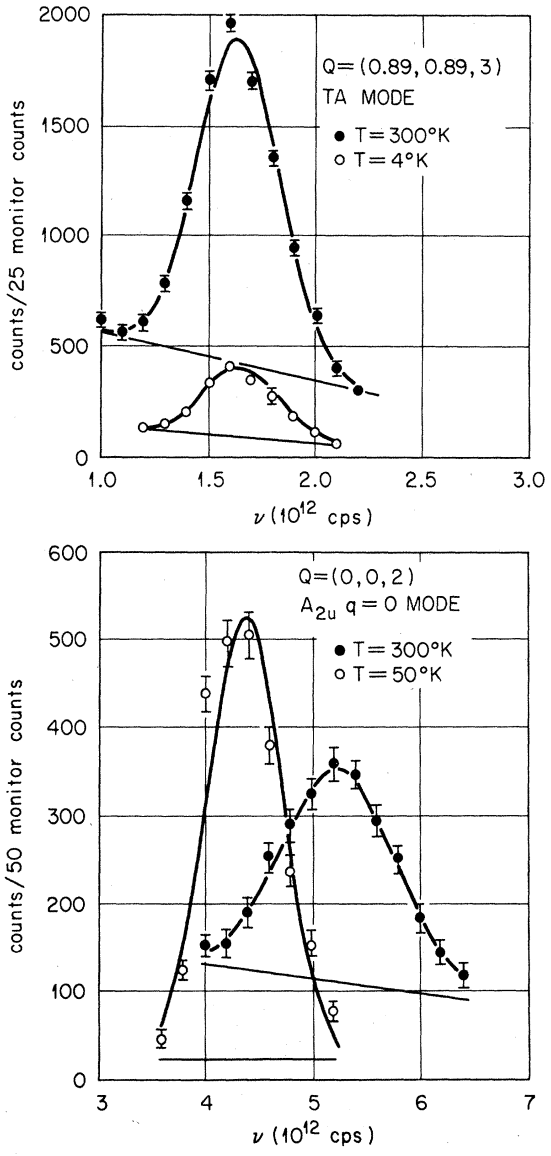

FIG. 13. Neutron groups of the $\Gamma_1^-(A_{2u})$ mode and TA $\Sigma_3(1)$ mode, measured at two temperatures.

The squares of measured frequencies are plotted versus temperature in Fig. 12, along with the squares of frequencies calculated from the static dielectric constant (c-axis) measurements of Parker by using Eq. (9) in the form

$$\nu_t^2(T) = \frac{\nu_l^2 \epsilon_{c,\infty}}{\epsilon_{c,0}(T)} = \frac{\text{const}}{\epsilon_{c,0}(T)} \,. \tag{15}$$

The constant was calculated from the $\epsilon_{c,0}$ (300 °K) of Parker and our ν_t^2 (300 °K). Determining a linear slope to the neutron data between 300 and 100 °K, we find a Curie temperature of − 540 °K [Eq. (11)] reflecting the fact that rutile does not become ferroelectric; however, a simple Curie law will not describe rutile since the data of Fig. 12 do not show a linear dependence on temperature.

Neutron groups of the $\Gamma_1^-(A_{2u})$ mode and the TA $\Sigma_2(1)$ mode are shown in Fig. 13. The intensity of the TA mode decreases by a factor of about 5, as is expected from the change of the phonon population factor in the coherent inelastic scattering cross section[40]; however, the intensity of the Γ_1^- mode increases with decreasing temperature. The asymmetry and abnormal increase of intensity of the Γ_1^- are both suggestive of the ionic displacements being increasing, causing increased anharmonicity in this mode at low temperatures.

V. SUMMARY

The phonon dispersion relation for rutile has been measured by the coherent inelastic scattering of thermal neutrons. Theoretical models based on the RIM and SM, with either axially symmetric or tensor first- and second-neighbor forces, have been constructed and fitted to the measured dispersion relations. Only the SM with tensor forces (as qualified in the text) was able to give qualitative agreement with the data, and that agreement is good for only some modes. Frequency distributions are calculated and presented, along with calculated Debye temperatures. The temperature dependence of the frequency of the $\Gamma_1^-(A_{2u})$ mode is measured, and the behavior of the square of the frequency is in good agreement with that predicted by the static dielectric constant measurements of Parker.

ACKNOWLEDGMENTS

The authors wish to express appreciation to N. Wakabayashi, M. E. Mostoller, R. F. Wood, and C. A. Rotter (University of West Virginia) for many helpful discussions and to J. L. Sellers for valuable experimental assistance. Gratitude is extended to G. W. Clark and R. A. Weeks for the loan of single-crystal samples, and to M. D. Beals of the National Lead Company, Titanium Division,

TABLE VII. Best-fit parameters of least-squares analysis of experimental dispersion curves.

Parameter	Quantity represented	Units	RIM III[a]	SM VII[a]
$P(1)$	ϕ_{xx} (11)	10^5 dyn/cm	0	0
$P(2)$	ϕ_{xy} (11)	10^5 dyn/cm	0	0
$P(3)$	ϕ_{zz} (11)	10^5 dyn/cm	0	0
$P(4)$	ϕ_{xx} (13)	10^5 dyn/cm	−0.7921	−0.0727
$P(5)$	ϕ_{xy} (13)	10^5 dyn/cm	−0.8924	−1.1165
$P(6)$	ϕ_{zz} (13)	10^5 dyn/cm	0.4051	0.5295
$P(7)$	ϕ_{xx} (23)	10^5 dyn/cm	−0.0809	−0.1363
$P(8)$	ϕ_{xy} (23)	10^5 dyn/cm	−0.0594	−0.6967
$P(9)$	ϕ_{xz} (23)	10^5 dyn/cm	0.6797	1.0053
$P(10)$	ϕ_{zx} (23)	10^5 dyn/cm	0.9127	1.1746
$P(11)$	ϕ_{zz} (23)	10^5 dyn/cm	−0.8288	−1.2100
$P(12)$	ϕ_r (34)	10^5 dyn/cm	−0.1751	−0.2673
$P(13)$	ϕ_t (34)	10^5 dyn/cm	0.0001	0.0289
$P(14)$	ϕ_{xx} (35)	10^5 dyn/cm	−0.7036	−0.7152
$P(15)$	ϕ_{xy} (35)	10^5 dyn/cm	−0.6432	−0.6500
$P(16)$	ϕ_{zz} (35)	10^5 dyn/cm	−0.5737	−0.4293
$P(17)$	Z (Ti)	dimensionless	2.1967	2.5215
$P(18)$[b]	Z (O)	dimensionless	−1.0984	−1.2608
$P(19)$	α (Ti)	Å^3	0	0.3578
$P(20)$	α (O)	Å^3	0	0.4832
$P(21)$	d (Ti)/e	dimensionless	0	0.0594
$P(22)$	d (O)/e	dimensionless	0	0.2487
	χ	dimensionless	9.9	7.8

[a]Parameters are given to four decimal places to allow accurate verification of the calculations. Number of digits is not intended to indicate significance (see text).

[b]$P(18)$ is constrained to be equal to $-\frac{1}{2}P(17)$.

for growing large, specially oriented samples. The authors are particularly grateful to R. S. Katiyar and G. S. Pawley of the University of Edinburgh, Scotland, for sending us their preliminary measurements on phonons in rutile. One of us (J. G. T.) wishes to express his appreciation to the Oak Ridge Associated Universities for a fellowship during this work, and to the Solid State Division, ORNL, for making his stay pleasant and rewarding.

*Research sponsored by the U. S. Atomic Energy Commission, under contract with the Union Carbide Corporation. Paper based on J. G. Traylor's doctoral dissertation, Dept. of Physics, University of Tennessee, 1971 (unpublished).

†Oak Ridge Graduate Fellow from the University of Tennessee under appointment from Oak Ridge Associated Universities. Present address: Dept. of Physics, Iowa State University, Ames, Iowa 50010.

[1]R. W. G. Wyckoff, *Crystal Structures*, 2nd ed. (Interscience, New York, 1963), Vol. II, p. 251.

[2]Preliminary measurements on MgF_2 have been made and reported by R. Kahn, J. P. Trotin, D. Cribier, and C. Bensit, in *Proceedings of the Fourth IAEA Symposium on Neutron Inelastic Scattering* (IAEA, Vienna, 1968), Vol. I, p. 289. Also, preliminary measurements of phonons in TiO_2 have been made by R. S. Katiyar and G. S. Pawley, University of Edinburgh, Edinburgh, Scotland (private communication). Measurements on CoF_2 are reported by P. Martel, R. A. Cowley, and R. W. H. Stevenson, Can. J. Phys. 46, 1355 (1968).

[3]F. A. Grant, Rev. Mod. Phys. 31, 646 (1959).

[4]S. P. S. Porto, P. A. Fleury, and T. C. Damen, Phys. Rev. 154, 522 (1967).

[5]P. S. Narayanan, Proc. Indian Acad. Sci. 32A, 279 (1950).

[6]W. G. Spitzer, R. C. Miller, D. A. Kleinman, and L. E. Howarth, Phys. Rev. 126, 1710 (1962).

[7]D. M. Eagles, J. Phys. Chem. Solids 25, 1243 (1964).

[8]J. B. Wachtman, Jr., W. E. Tefft, and D. G. Lam, Jr., J. Res. Natl. Bur. Std. 66A, 465 (1962).

[9]G. L. Vick and L. E. Hollander, J. Acoust. Soc. Am. 32, 947 (1960).

[10]R. A. Parker, Phys. Rev. 124, 1719 (1961).

[11]W. Cochran, Advan. Phys. 9, 387 (1960).

[12]B. Dayal, Proc. Indian Acad. Sci. 32A, 304 (1950).

[13]A. I. Gubanov and M. S. Shur, Fiz. Tverd. Tela 7, 2626 (1965) [Sov. Phys. Solid State 7, 2124 (1966)].

[14]R. S. Katiyar and R. S. Krishnan, Phys. Letters 25A, 525 (1967).

[15]M. Born and K. Huang, *Dynamical Theory of Crystal Lattices* (Oxford U. P., New York, 1954).

[16]E. W. Kellermann, Phil. Trans. Roy. Soc. London A238, 513 (1940).

[17]R. A. Cowley, Acta Cryst. 15, 687 (1962).

[18]G. Leibfried and W. Ludwig, Solid State Phys. 12, 275 (1961).

[19]G. Dolling, in *Molecular Dynamics and Structure of Solids*, edited by R. S. Carter and J. J. Rush, Special Publication 301 (Natl. Bur. Std., Washington, D. C., 1969), p. 289.
[20]B. G. Dick and A. W. Overhauser, Phys. Rev. 112, 90 (1958).
[21]B. Szigeti, Trans. Faraday Soc. 45, 155 (1949).
[22]A. D. B. Woods, W. Cochran, and B. N. Brockhouse, Phys. Rev. 119, 980 (1960).
[23]R. A. Cowley, W. Cochran, B. N. Brockhouse, and A. D. B. Woods, Phys. Rev. 131, 1030 (1963).
[24]W. Cochran, R. A. Cowley, G. Dolling, and M. M. Elcombe, Proc. Roy. Soc. (London) A293, 433 (1966).
[25]P. R. Vijayaraghavan, R. M. Nicklow, H. G. Smith, and M. K. Wilkinson, Phys. Rev. B 1, 4819 (1970).
[26]S. H. Chen, Phys. Rev. 163, 532 (1967).
[27]J. G. Gay, W. A. Albers, Jr., and F. J. Arlinghaus, J. Phys. Chem. Solids 29, 1449 (1968).
[28]R. S. Katiyar, J. Phys. C 3, 1087 (1970).
[29]W. Cochran, Z. Krist. 112, 465 (1959).
[30]A. S. Barker, Jr., Phys. Rev. 136, A1290 (1964).
[31]M. K. Wilkinson, H. G. Smith, W. C. Koehler, R. M. Nicklow, and R. M. Moon, in *Proceedings of the Fourth IAEA Symposium on Neutron Inelastic Scattering* (IAEA, Vienna, 1968), Vol. II, p. 253.
[32]P. K. Iyengar, in *Thermal Neutron Scattering*, edited by P. A. Egelstaff (Academic, London, 1965), p. 98.
[33]G. Gilat and L. J. Raubenheimer, Phys. Rev. 144, 390 (1966).
[34]M. E. Mostoller (private communication).
[35]T. R. Sandin and P. H. Keesom, Phys. Rev. 177, 1370 (1969).
[36]J. S. Dugdale, J. A. Morrison, and D. Patterson, Proc. Roy. Soc. (London) 224A, 228 (1954).
[37]C. H. Shomate, J. Am. Chem. Soc. 69, 218 (1947).
[38]H. N. Pandey, Phys. Status Solidi 11, 743 (1965).
[39]J. R. Tessman, A. H. Kahn, and W. Shockley, Phys. Rev. 93, 890 (1953).
[40]W. M. Lomer and G. G. Low, in *Thermal Neutron Scattering*, edited by P. A. Egelstaff (Academic, London, 1965), p. 1.

PHYSICAL REVIEW B VOLUME 3, NUMBER 10 15 MAY 1971

Phase Transition in a Wigner Lattice*

Leslie L. Foldy
Department of Physics, Case Western Reserve University, Cleveland, Ohio 44106
(Received 21 December 1970)

Detailed calculations of the frequency spectrum of lattice vibrations for the body-centered-cubic and face-centered-cubic Wigner lattices in the harmonic approximation show that a phase transition from the body-centered-cubic to either the face-centered-cubic lattice or to some other lattice almost certainly occurs with increasing temperature at sufficiently low densities, but a transition from the body-centered-cubic to the face-centered-cubic lattice does not occur at zero temperature with increasing density in the region where the harmonic approximation is valid. The parameterless frequency spectra for the two lattices, which have been calculated to relatively high accuracy, and their moments are tabulated.

I. INTRODUCTION

The problem of a many-body system consisting of identical point-charged particles moving in a compensating rigid uniform background of opposite charge was first studied as a model for the electron gas in a solid. At zero temperature (or sufficiently low temperatures) and very high densities, the system behaves as a degenerate Fermi gas, and hence is a fluid. In the high-density expansion of the zero-temperature energy of such a system, the leading terms are the Fermi energy and the exchange energy associated with the Coulomb interaction. The next two terms in the expansion were first obtained by Gell-Mann and Brueckner[1] and are the leading terms in what is called the correlation energy of the system. An early attempt to estimate the correlation energy of the electron gas, particularly at intermediate densities, led Wigner[2] to examine the low-density limit of the same system and to discover that in this limit such a system (whether composed of fermions or bosons) crystallizes in the classical configuration of minimum potential energy which, by all indications, appears to be a body-centered-cubic (bcc) lattice. Thus, as a function of density, even at zero temperature, a fermion system of this type must undergo a phase transition from a crystalline to a fluid phase. A similar situation seems to prevail for boson systems at zero temperature since the high-density behavior is predicted to be that of a superfluid.[3] Furthermore, the elementary excitations of the high-density boson system appear to be plasma oscillations (plasmons) with a finite energy gap separating them from the ground state, while the low-energy excitations of the low-density Wigner lattice are phonons with no energy gap. Thus there must be a transition density at which the finite gap disappears.

Since Wigner's original exploration of the so-